Single photon radioluminescence

I. Theory and spectroscopic properties

S. Bicknese, Zahra Shahrokh, Stephen B. Shohet, and A. S. Verkman

Departments of Laboratory Medicine, and Medicine and Physiology, Cancer Research Institute and Cardiovascular Research Institute, University of California, San Francisco, California 94143 USA

ABSTRACT The excitation of a fluorescent molecule by a beta-decay electron (radioluminescence) depends upon the electron energy, the distance between radioactive 'donor' and fluorescent 'acceptor', and the excitation characteristics and solvent environment of the fluorophore. The theory for calculation of single photon radioluminescence (SPR) signals is developed here; in the accompanying paper, measurement methods and biological applications are presented. To calculate the three-dimensional spatial profile for electron energy deposition in an aqueous environment, a Monte Carlo calculation was performed incorporating theories of electron energy distributions, energy loss due to interactions with matter, and deflections in electron motion due to collisions. For low energy beta emitters, 50% of energy deposition occurs within 0.63 μm (^{3}H, 18.5 keV), 22 μm (^{14}C, 156 keV), 25 μm (^{35}S, 167 keV), and 260 μm (^{36}Cl, 712 keV) of the radioisotope. In close proximity to the beta emitter (100 nm, ^{3}H; 10 μm, ^{14}C) the probability for fluorophore excitation is approximately proportional to the inverse square of the distance between the beta emitter and fluorophore. To investigate the other factors that determine the probability for fluorophore excitation, SPR measurements were carried out in solutions containing ^{3}H and a series of fluorophores in different solvents. In water, the probability of fluorescence excitation was nearly proportional to the integrated absorbance over a >1,000-fold variation in absorbances. The probability of fluorescence excitation was enhanced up to 2,600-fold when the fluorophore was in a "scintillant" aromatic or hydrocarbon solvent. SPR emission spectra were similar to fluorescence emission spectra obtained with photon excitation. The single photon signal due to Bremsstrahlung increased with wavelength in agreement with theory. The distance dependence for the SPR signal predicted by the model was in good agreement with measurements in which a ^{14}C donor was separated by known thicknesses of water from a fluorescently-coated coverglass. Quantitative predictions for radioluminescence signal as a function of donor-acceptor distance were developed for specific radioisotope-fluorophore geometries in biological samples.

INTRODUCTION

The electrokinetic energy contained in an electron emitted by a decaying radioisotope can be used to excite fluorescence in a reporter fluorophore. This principle has been used extensively to measure radioactivity in biological samples by scintillation spectrometry. In conventional measurements of radioactivity, the radioisotope is immersed in a concentrated solution of fluorophore in a "scintillant" solvent which enhances the efficiency of fluorophore excitation. Under these conditions, a beta electron excites many fluorophores to give a substantial flash of light consisting of many photons moving in multiple random directions. To maximize the detected signal relative to background noise, the light flash is detected by two photomultipliers in a coincidence mode. As described in this and the accompanying manuscript, the extension of (multi-photon) scintillation spectrometry to a single beta-emitting radioisotope and a single reporter fluorophore provides a novel and potentially powerful approach to examine a variety of biological questions related to submicroscopic distance determination, receptor-ligand binding, membrane transport, and lipid dynamics.

The central principle in what is herein called 'single photon radioluminescence' (SPR) is that the excitation of a reporter fluorophore depends on the distance between the "donor" beta-emitter and the "acceptor" fluorophore. In SPR, in contrast to conventional scintillation spectroscopy, at most a single photon is detected from each radioactive decay. The concept of donor and acceptor stems from usage in fluorescence resonance energy transfer (RET); however, as described below, the information derived from SPR measurements is inherently different from, and complementary to, that derived from RET studies. There have been remarkably few applications which make use of the distance information available in radioluminescence measurements. Von Tscharner and Radda (1980, 1981) first described radioluminescence measurements in condensed lipid phases and showed that the radioluminescence signal was sensitive to the physical state of the lipid suspensions. Although the possibility of novel biological applications was proposed, there have been no further reports of single photon radioluminescence measurements in the past decade. Other general applications of (multiphoton) radioluminescence include: a "proximity" assay for antibody binding in which the decay of ^{125}I or ^{3}H excites fluorescence when bound to a bead containing fluorophores immobilized in a polymeric matrix (Bosworth and Towers, 1989), and a permanently lit radioluminescent light bulb in which a fluorophore and an intense radioactive source are embedded in a matrix having scintillant properties (Renschler and Clough, 1989).

The purpose of this and the accompanying paper is to establish a rigorous foundation for application of SPR to biochemical and cellular systems. In this paper, we report the theory for quantitative analysis of SPR signals

Address correspondence to Stephen Bicknese, Ph.D., MacMillan-Cargill Hematology Research Laboratory, 1217 Health Sciences East, University of California, San Francisco, CA 94143-0134.

0006-3495/92/11/1256/11 $2.00

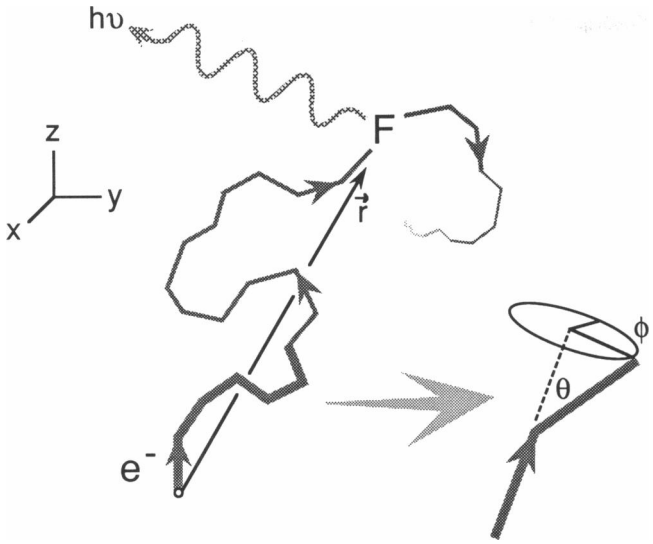

FIGURE 1 Fluorescence excitation by beta decay. Schematic showing the trajectory of an electron as it deposits energy and undergoes multiple scattering events during passage through aqueous media. Emission of a photon ($h\nu$) by a fluorophore (F) in the electron path is shown. Each scattering event is defined by a deflection angle (θ) and an azimuthal angle (ϕ). See text for details.

and a set of measurements to validate the theory and to evaluate important spectroscopic properties. In the accompanying paper, we report the SPR detection apparatus and examine the special requirements for SPR measurements in biological samples. In addition, based on the theoretical and experimental developments, several novel biological applications will be presented.

THEORY

Overview

The purpose of the theory is to calculate the SPR signal (in fluorescence cps) for a sample containing beta emitters and reporter fluorophores distributed in a specified geometry. Fig. 1 shows the decay of a radioisotope producing an electron which travels in a random initial direction with some given initial kinetic energy. For each radioisotope there is a continuous distribution of initial energies up to a maximum energy. The ejected electron undergoes a series of interactions with molecules in the aqueous environment resulting in deflections in its three-dimensional path and local deposition of energy. If a fluorophore is at or very near the electron path, there is a finite probability for fluorophore excitation given by an interaction cross-section. The fluorophore decay may produce a photon (probability given by the fluorescence quantum yield), whose detection efficiency depends upon the geometric probability that the photon reaches the detector and the detector quantum efficiency. Additional considerations are the production of photons in the absence of fluorophores ("stopping radiation" or Bremsstrahlung) and the effect of the fluorophore environment on the cross-section for excitation (scintillant effect, see below).

Monte Carlo calculation

The spatial distribution of energy deposition for an electron produced by beta decay was calculated by a Monte Carlo simulation. The continuous-slow-down approximation (Berger and Seltzer, 1982) was applied to calculate the rate of energy loss ($-dE/dx$, keV/cm) during passage of mono-energetic electrons through the aqueous medium. According to the relativistic Bethe equation (Bethe and Ashkin, 1953; Mladjenovic, 1973);

$$-dE/dx = 153\rho(Z/A)\beta^{-2}B, \tag{1}$$

where

$$B = \ln [Em_0c^2\beta^2/(2I^2(1-\beta)^2)] - [2(1-\beta^2) - 1 + \beta^2] \times \ln 2 + 1 - \beta^2 + 0.125[1-(1-\beta^2)^{1/2}]^2. \tag{2}$$

ρ is the media density ($\sim$1 g/cm^3 for aqueous media) and Z, A, and I are the effective atomic number, atomic mass, and ionization energy of the absorbing aqueous medium, taken to be 7.23, 14.3, and 75 eV, respectively (Rossi, 1952; Berger and Seltzer, 1982). m_0c^2 is the rest energy of an electron (511 keV) and β is the ratio of electron velocity to the speed of light (v/c) determined relativistically from the electron kinetic energy E,

$$\beta = [1-(1+E/m_0c^2)^{-2}]^{1/2}. \tag{3}$$

The electron loses energy continuously as it travels through the aqueous medium. For purposes of the Monte Carlo calculation as proposed by Berger (1963), specified "energy deposition" steps are chosen to track the position of the electron along its path. If E_n is the kinetic energy of the electron at step n, then E_{n+1} is taken to be $2^{-1/m}E_n$, producing a decreasing geometric progression of kinetic energies where half of the initial electron energy is lost in m steps (m = 32 in calculations here). This discrete spacing of energies produces a discrete spacing of successive particle positions,

$$2^{-1/m} = 1 - \frac{1}{E_n}\int_{S_n}^{S_{n+1}} \left|\frac{dE}{dx}\right| dS, \tag{4}$$

where S_n is the cumulative distance (along the actual convoluted path) traveled by the electron from its origin. S_{n+1} was calculated from S_n by the relation,

$$S_{n+1} = [(1-2^{-1/m})E_n + S_n\langle dE/dx\rangle]/\langle dE/dx\rangle, \tag{5}$$

where $\langle dE/dx\rangle$ is the average energy loss over the interval between positions S_{n+1} and S_n.

The positions of the electron during its movements in three-dimensions (x_n, y_n, z_n) are next considered. The electron undergoes multiple scattering events resulting in a series of deflections. For an energy step E_n to E_{n+1},

the net angle of deflection, θ_n, (from its previous direction) is described approximately by the relation (Blanchard and Fano, 1951),

$$\langle \cos \theta_n \rangle \cong [(E_{n+1}/E_n)(E_n + 2m_0c^2)/(E_{n+1} + 2m_0c^2)]^{0.3Z}. \quad (6)$$

An advantage of choosing a geometric progression for energy spacings is that the scattering angles, θ_n, do not change appreciably with successive steps. The angle for each step depends upon the ratio of the beginning and ending energy as determined by the geometric progression.

To carry out the Monte Carlo calculation, random numbers are generated at step n to specify the deflection in electron path (see Fig. 1). The scattering angle, θ_n, is a Gaussian distributed random number with an average angle $\langle \theta_n \rangle$ and standard deviation $2^{-0.5}\theta_n$ (Berger, 1963; Demas, 1983). An azimuthal angle, ϕ_n, is chosen as a uniformly distributed random number between 0 and 2π. The pathlength at each step ($\Delta S_n = S_{n+1} - S_n$), the electron position at step n, and the scattering angles (ϕ_n and θ_n) are used to determine the electron position at step $n + 1$ by a product of rotation matrices $\mathbf{R}$ (which rotates the deflected path of the electron into the fixed laboratory x, y, z frame),[1]

$$\begin{pmatrix} x_{n+1} \\ y_{n+1} \\ z_{n+1} \end{pmatrix} = \begin{pmatrix} x_n \\ y_n \\ z_n \end{pmatrix} + \mathbf{R}_1 \cdot \mathbf{R}_2 \cdot \mathbf{R}_3 \cdot \cdots \mathbf{R}_n \begin{pmatrix} 0 \\ 0 \\ \Delta S_n \end{pmatrix}, \quad (7)$$

where $\mathbf{R}_n$ is defined by,

$$\mathbf{R}_n = \begin{pmatrix} \cos\theta_n \cos\phi_n & -\sin\phi_n & \sin\theta_n \cos\phi_n \\ \cos\theta_n \sin\phi_n & \cos\phi_n & \sin\theta_n \sin\phi_n \\ -\sin\theta_n & 0 & \cos\theta_n \end{pmatrix}. \quad (8)$$

The spatial distribution of energy deposited by monoenergetic electrons initially moving in the z-direction was calculated on an Intel 486 cpu. Generally, the paths for 10^4 electrons were calculated at each energy ($\sim$120 min cpu time); each path contained up to 200 scattering steps so that final E was <0.5 keV (see Discussion). Because of the cylindrical symmetry for energy deposition around the z-axis, energy depositions were accumulated in a two-dimensional array with position coordinates z and r, where r is the perpendicular distance from the z-axis ($r^2 = x^2 + y^2$).

The calculation above gives the spatial distribution for energy deposition [$D_E(z, r)$, units keV/cm^3] by monoenergetic electrons with initial kinetic energy E, whose spatial integral (over $r\,dr\,dz$) equals E. To calculate the energy deposition by beta decay in radioisotope x [$D_x(z, r)$], the spatial distribution for monoenergetic electrons is convoluted with the spectrum of initial electron energies, $N(E)dE$. $N(E)dE$ was derived from expressions given in Evans (1955).

$$N(E)dE = 64\pi^4 g/h^7c^2 |P|^2 F(Z', E) \times (E + m_0c^2)(E_0 - E)^2/(E^2 + 2Em_0c^2)^{0.5}dE, \quad (9)$$

where g is the Fermi constant ($\sim 10^{-49}$ cm^2·ergs), $h/2\pi m_0 c$ is the Compton wavelength of an electron (3.86×10^{-11} cm), $|P|^2$ is the squared modulus of the transition matrix ($\sim$1), and E_0 is the maximum electron kinetic energy (e.g., E_0 = 18.5 keV for ^{3}H; 156 keV for ^{14}C; 167 keV for ^{35}S). $F(Z, E)$ is a correction factor which takes into account the nuclear coulomb potential (Evans, 1955). The nonrelativistic approximation, $F(Z, E) = 2\pi Z'/[137\beta(1 - e^{-2\pi Z'/137\beta})]$, is valid for electron energies < 511 keV. β is calculated from E by Eq. 3, and Z' is the nuclear charge after beta decay. $D_x(z, r)$ was calculated by numerical convolution of $D_E(z, r)$ with $N(E)dE$. The spatial integral of $D_x(z, r)$ (over $r\,dr\,dz$) is the average electron energy for radioisotope x. For numerical convolution, $D_E(z, r)$ was generated for 0.5, 5.0, and 20 keV increments in E by the Monte Carlo method for ^{3}H, ^{14}C, and ^{36}Cl, respectively.

Calculation of radioisotope-fluorophore distances

The function $D_x(z, r)$ can be used to predict SPR signals for relevant geometries encountered experimentally. For decay of a radioisotope in which the initial electron direction is random, the energy deposited at a distance $R = [z^2 + r^2]^{0.5}$ from the radioactive donor, $D'_x(R)$, is determined by integration of $D_x(z, r)$, expressed in polar coordinates [$D'_x(R, \theta) = D_x(R \sin\theta, R \cos\theta)$], over the polar angle θ. The spatial integral of $D'_x(R)$ (over $4\pi R^2\,dR$) is the average electron energy for radioisotope x. For an arbitrary spatial distribution of fluorescent acceptors, $S(R)$ (fluorophores/cm^3), the number of excited fluorophores produced per unit time, $N^*[S(R)]$, in sample volume V (cm^3) is given by,

$$N^*[S(R)] = 4\pi A_r V \sigma_F \int D'_x(R) S(R) R^2\,dR, \quad (10)$$

where σ_F is an apparent cross-section (excited fluorophores·cm^3·fluorophore^{-1}·$\langle$keV$\rangle^{-1}$·μCi^{-1}·s^{-1}) relating energy deposition to fluorescence excitation (see below), and A_r (μCi) is the number of radioisotope decays per unit time determined by the product of radioisotope specific activity (μCi/mmol), concentration (mmol/cm^3), and sample volume.

For a uniform distribution of fluorophores in solution, $S(R) = \rho_F$ (fluorophore density in units of fluorophores/cm^3); Eq. 10 predicts that $N^* = \sigma_F A_r V \rho_F \langle E_x \rangle$, where

[1] In Eqs. 7 and 8, an electron at step n moves a distance ΔS_n along the z'-axis in an x', y', z' reference frame. The components of ΔS_n in the laboratory frame are determined by serial rotations of vector $(x', y', z') = (0, 0, \Delta S_n)$ from the x', y', z' frame back through each previous reference frame (as defined by electron direction). Each rotation is accomplished by a rotation matrix $\mathbf{R}_n$ which includes polar and azimuthal Euler angles (Marion, 1971).

$\langle E_x \rangle$ is the average electron energy density (keV/cm^3) for radioisotope x. For point-to-point geometry in which radioactive donors and fluorescent acceptors are separated by a fixed distance R_0, $S(R) = n_F\delta(R - R_0)/4\pi R_0^2$, where n_F is the number of fluorophores that are located at a distance R_0 from each donor and thus can serve as potential acceptors; N^* then becomes $\sigma_F A_r n_F D'_x(R_0)$. For point-to-plane geometry in which fluorophores are distributed in a plane at a distance R_0 from the radioactive donor, $S(R) = \rho_F h(R - R_0)/R$, where ρ_F is the fluorophore planar density (fluorophore/cm^2) and $h(R - R_0)$ is the stepfunction ($h(R - R_0) = 0$ for $R < R_0$, and 1 for $R > R_0$). For point-to-line geometry in which fluorophores are distributed along a line at a distance R_0 from the radioactive donor, $S(R) = \rho_F h(R - R_0)/[R^2(1 - R_0^2/R^2)^{0.5}]$, where ρ_F is the fluorophore linear density (fluorophore/cm). For point-to-plane and point-to-line geometry, N^* is calculated from $D'_x(R)$ and $S(R)$ by Eq. 10.

The detected SPR signal (L_{rad}, in counts per second, cps) is related to the number of excited fluorophores per second, $N^*[S(R)]$, by,

$$L_{rad} = N^*[S(R)]I_a(\lambda)Q_yGQ_e(\lambda), \qquad (11)$$

where $I_a(\lambda)$ is an inner-filter correction resulting from the absorption of emitted photons, Q_y is fluorophore quantum yield (photons/excited fluorophore), G is a dimensionless geometric factor representing the probability that an emitted photon reaches the detector, and $Q_e(\lambda)$ is the wavelength-dependent detector quantum efficiency (cps/photons).

Eqs. 10 and 11 provide an experimental strategy to determine distances between radioactive donor and fluorescent acceptor. L_{rad} and Q_y are measured. $D'_x(R)$ is obtained from the Monte Carlo calculations. The product $\sigma_F GQ_e(\lambda)$ is determined from a "normalization" experiment in which radioluminescence is measured for a uniform distribution of fluorophores and radioisotopes in solution (see Results). V and A_r are known. Finally, assuming a functional form for $S(R)$, the unknown distance can be calculated. Examples of biologically important forms for $S(R)$ as given above are point-to-point geometry (e.g., distance between labeled membrane skeletal proteins) and point-to-plane geometry (e.g., distance between lipid membrane bilayer and membrane skeletal protein).

EXPERIMENTAL METHODS

Fluorescent compounds were purchased from Molecular Probes Inc. (Junction City, OR). Spectroscopic grade solvents, PVC, and plasticizer were purchased from Aldrich Chemical Co. (Milwaukee, MI). Radioisotopes were purchased from Amersham (Arlington Heights, IL).

The apparatus for measurement of radioluminescence signals is described in detail in the accompanying manuscript (Shahrokh et al., 1992). Samples were contained in 0.7 ml cylindrical glass vials. For spectral studies, a series of Schott glass cut-on filters (Duryea, PA) were interposed between the sample and detector. Radioluminescence signals were corrected for inner filter effect and photomultiplier efficiency as described in the accompanying manuscript. Fluorophore quantum yield was measured on an SLM 8000C fluorimeter (Urbana, IL) and absorbance spectra on a Hewlett Packard photodiode array spectrometer.

For distance measurements, 12-mm round glass coverslips were coated with a 1–2-μm thickness of polyvinylchloride (PVC) containing either ^{14}C-palmitic acid or 12 (9-anthroyloxy) stearic acid. The coating was applied by dipping acid washed coverslips in a solution of PVC (4.8 mg/ml) and tris(2-ethylhexyl) phosphate plasticizer (14.4 mg/ml) in 3:1 mixture tetrahydrofuran:ethyl ether containing the radioisotope or fluorophore. Radioluminescence was measured in "sandwiches" with various thicknesses of water interposed between the radioactive and fluorescent coverglasses (PVC surface facing inward).

RESULTS

Representative results of the Monte Carlo calculation for monoenergetic electrons ejected initially in the z-direction are shown in Fig. 2. Trajectories for a series of electrons are shown at the left as a two-dimensional projection of the calculated three-dimensional path. Note the increased axial and lateral electron penetration at higher initial energies.

The data on the right have been expressed as iso-absorption plots, where contours indicate the fractions of energy absorbed at specified positions. The iso-absorption contours in three-dimensions are cylindrically symmetrical around the z-axis. For absorption of electron energy in aqueous media, the distance over which energy is distributed increases remarkably with increased initial electron energy. For electrons ejected initially in the z-direction, most of the energy is deposited in the forward direction and at significant lateral distances from the z-axis due to multiple scattering events. The range of the forward and lateral energy deposition increases with particle energy, but the ratio of forward and lateral range (contour shape) remains nearly the same. To examine the effect of energy step size on model predictions, the iso-absorption plots in Fig. 2 were recalculated for a five-fold increase in the number of steps. For a simulation involving the trajectories of 10^4 electrons, the $D_E(z, r)$ values and derived fractions of energy remaining at each point in the z-r plane agreed to within 2% of those calculated for the array used to generate Fig. 2.

Data from multiple monoenergetic electrons were superimposed to calculate the spatial profile for energy deposition by electrons from ^{3}H and ^{14}C ejected in the z-direction. Fig. 3 *A* shows the continuous distribution of energies for electrons from ^{3}H and ^{14}C, and for comparison, higher energy electrons from ^{36}Cl. The electron energy spectra are broad because of the requirement for momentum conservation for the electron and antineutrino that are produced in beta decay. Fig. 3, *B* and *C* show the iso-absorption plots for ^{3}H and ^{14}C. Compared with the data shown for monoenergetic electrons in Fig. 2, the superposition of data for the continuous distribution of electron energies shows a different spatial distri-

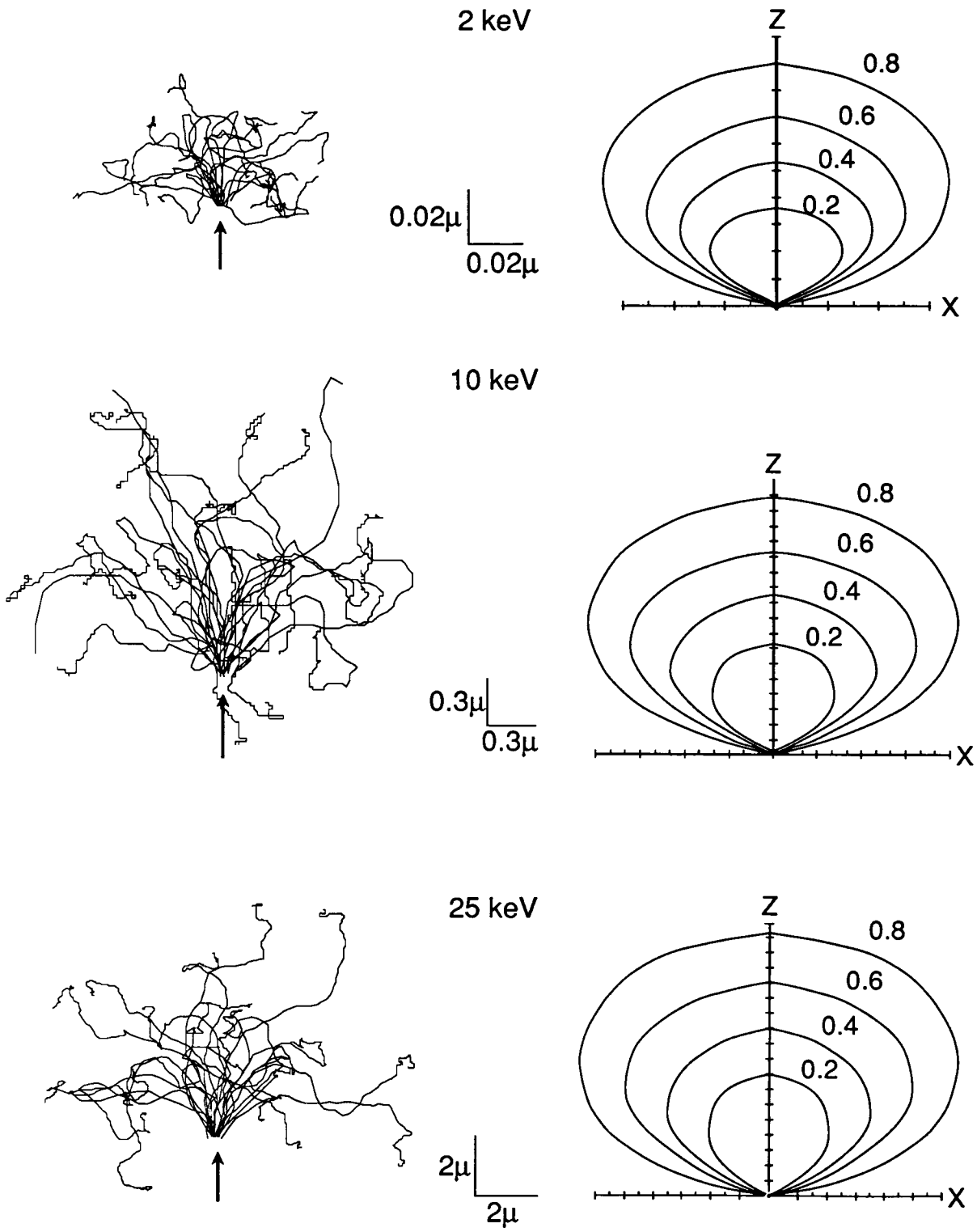

FIGURE 2 Iso-absorption plots for monoenergetic electrons elected along the z-axis. Plots were obtained from the Monte Carlo calculation described in the Theory section. (A) Representative trajectories for individual electrons for three different initial electron energies. Motions only in the x-z plane are shown. (B) Iso-absorption contour plots. Each contour defines the area in which the indicated fraction of electron energy is absorbed. Note that contours represent a planar section through a three-dimensional surface with cylindrical symmetry around the z-axis.

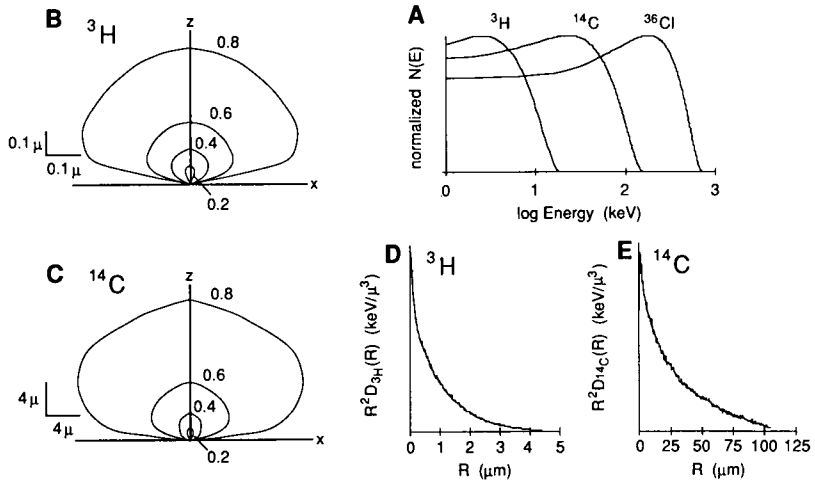

FIGURE 3 Deposition of energy by beta electrons produced by ^{3}H and ^{14}C. (*A*) Spectrum of initial electron kinetic energies calculated by Eq. 9. (*B* and *C*). Iso-absorption plots for ^{3}H and ^{14}C electrons calculated by the superposition of energy deposition data for monoenergetic electrons, weighted according to the energy spectrum $N(E)$ given in *A*. (*D* and *E*) Deposition of electron energy as a function of radial distance (R) from the isotope. The ordinate $R^2D_x(R)$ was calculated as described in Theory. See text for details.

bution for energy deposition with a gradual decline at large distances. For ^{14}C (maximum electron energy 156 keV), the distances over which electron energy is deposited are appreciably greater than those for ^{3}H (maximum electron energy 18.5 keV).

In an actual beta decay, the electron is ejected from the nucleus in a random direction. As described in the Theory section above, the function $D_x(R)$ was generated to quantify the dependence of energy deposition, in units of keV/cm^3, on the radial distance R from the radioisotope. The $D_x(R)$ plots (Fig. 3, (*D* and *E*) show that ~50% of initial electron energy is deposited within 0.63 μm for ^{3}H and 22 μm for ^{14}C. Another useful radioisotope for experimental radioluminescence measurements is ^{35}S (maximum electron energy 167 keV) which gives similar $D_x(R)$ to that of ^{14}C. Note that $R^2D_x(R)$ for ^{3}H remains relatively constant for $R < 100$ nm, implying that the deposition of electron energy in a fixed volume (e.g., for fluorophore excitation) falls approximately as $1/R^2$. The $1/R^2$ dependence is expected for a point radiation source.

The calculations above provide information about the spatial distribution for energy deposition. The physical processes by which the deposited energy is transduced into fluorescence excitation are less well understood. To investigate the physical characteristics of a fluorescent molecule that are important for excitation by a moving electron, radioluminescence intensities were measured for a series of fluorophores having widely differing properties. Measured radioluminescence signals (in cps) were corrected for detector efficiency and fluorophore quantum yield so that measured cps are proportional to the cross-section (σ_F, see Eq. 10) for fluorescence excitation. Fig. 4 shows a series of measurements for fluorophores in nonscintillating solutions containing 10 μCi ^{3}H-glucose. Initial comparisons showed little correlation between σ_F and emission or excitation wavelengths, quantum yield, molecular dimensions, and dielectric properties. Interestingly, there was a very good correlation between σ_F and the wavelength-integrated fluorophore absorption spectrum. This correlation held for a three order of magnitude range in integrated absorption, from 2×10^5 M^{-1} cm^{-1} nm for tryptophan, to 2×10^8 M^{-1} cm^{-1} nm for β-phycoerythrin. The data were fitted to the empirical equation $\sigma_F = 5.06 \times 10^{-27} [\int \epsilon(\lambda)\, d\lambda]^{1.13}$, where σ_F is expressed in units of excited fluorophores · cm^3 · fluorophore^{-1} · $\langle$keV$\rangle^{-1}$ · μCi^{-1} · s^{-1} and $\int \epsilon(\lambda)\, d\lambda$ in units of M^{-1} cm^{-1} nm. Further experiments were carried out to investigate the nature of the transition(s) accounting for the radioluminescence signals.

Fig. 5 shows emission spectra for radioluminescence signals measured by interposing a series of low phosphorescence cut-on filters between the sample vial and detector. Fig. 5 *A* shows the fluorescence emission spectrum for fluorescein obtained by photon excitation, and the radioluminescence spectra obtained by ^{3}H and ^{14}C excitation (*dashed curves*). The close agreement in spectral shape suggests that the primary electronic transition accounting for the radioluminescence signal is the usual S_1 to S_0 transition for fluorescence emission. Spectra were also obtained for SPQ (Fig. 5 *B*), a fluorophore with a different emission spectrum. Again, there was good agreement in the shapes of the fluorescence and radioluminescence spectra.

The major source of background signal in radioluminescence measurements is the production of photons by the process of Bremsstrahlung or "stopping radiation" (Bethe and Ashkin, 1953). Theoretically, for a continuous distribution of electron energies, the intensity due to Bremsstrahlung is predicted to decrease with increasing

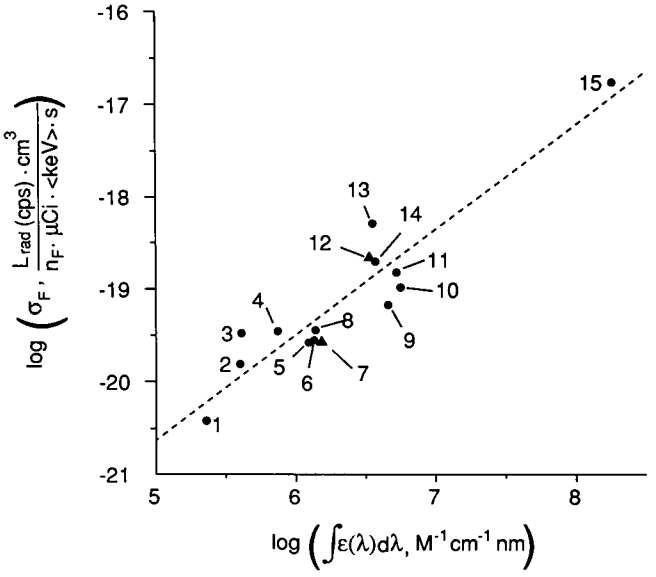

FIGURE 4 Relationship between the probability of excitation of fluorophores by ^3H and the wavelength-integrated fluorophore molar absorbance. Solutions contained 10 μCi ^3H-glucose and a range of fluorophore concentrations in aqueous buffers (*solid circles*) or ethanol (*solid triangles*). The abscissa is the log of the wavelength-integrated area under the fluorophore absorption peak ($M^{-1}\,cm^{-1}\,nm$) measured for fluorophore concentrations giving peak absorbances of <0.4 OD units at 1-cm pathlength. The ordinate is the log of the calculated SPR cross-section for fluorescence excitation (σ_F, see Eq. 10), determined from the measured radioluminescence signal (L_{rad}), corrected for $I_a(\lambda)$, G, Q_y, and $Q_e(\lambda)$ (see Eq. 11). Legend: (*1*) tryptophan; (*2*) 5-(2-((iodoacetyl)amino)ethyl)amino-naphthalene-1-sulfonic acid (IAEDANS); (*3*) 6-methoxy-[3-sulfopropyl] quinolinium (SPQ); (*4*) sulfopropylacridinium (SPA); (*5*) acridine orange; (*6*) 7-hydroxy-4-methylcoumarin (7 HMC); (*7*) terphenyl; (*8*) pyranine; (*9*) fluorescein (*10*) 3,3-dihexyloxacarbocyanine iodide (diOC(6)3); (*11*) rhodamine 6G; (*12*) diphenylhexatriene (DPH); (*13*) eosin-5-isothiocyanate; (*14*) 4,4'-diisothiocyanano-2,2'-disulfonic stilbene (DIDS); (*15*) β-phycoerythrin. The log–log data were fitted to a line with slope 1.13 and correlation coefficient 0.936.

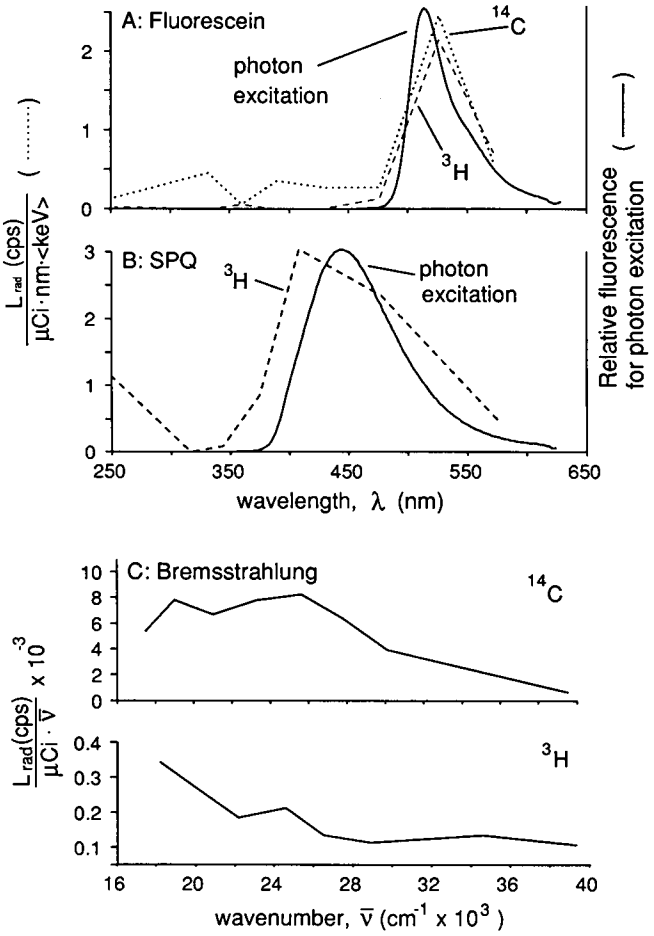

FIGURE 5 Wavelength dependence of radioluminescence signals. Radioluminescence signal (L_{rad}; cps · μCi^{-1} · $\langle keV \rangle^{-1}$ · nm^{-1}) as a function of wavelength for solutions consisting of: 200 μCi ^3H-glucose or 20 μCi ^{14}C in 10 mM Na phosphate in water (pH 8) containing 50 μM fluorescein (*A*), or 1 mM SPQ (*B*). Spectral intensities were determined by subtraction of SPR signals measured with filters having different cut-on wavelengths and normalized for the wavelength interval between filters. Data are corrected for detector efficiency [$Q_e(\lambda)$], and average electron energy ($\langle keV \rangle$) of the radioisotope. Solid curves in *A* and *B* are corrected fluorescence emission spectra measured by conventional cuvette fluorimetry with photon excitation at 460 and 350 nm, respectively. The curves in *C* are the single photon signals (L_{rad}; cps · μCi^{-1} · $wavenumber^{-1}$) arising from Bremsstrahlung as a function of wavenumber. Solutions contained 20 μCi ^{14}C-urea or 200 μCi ^3H-water in water. Data are corrected for detector efficiency [$Q_e(\lambda)$].

photon energy (wavenumber) (Evans, 1955); however, there has been no direct experimental support for this prediction. The measurement in Fig. 5 *C* was carried out in an aqueous buffer containing 200 μCi ^3H-water or 20 μCi ^{14}C-urea in the absence of fluorophore. The Bremsstrahlung spectrum shows a decrease in signal with increasing wavenumber in good agreement with theory (Evans, 1955).[2] Bremsstrahlung intensity is also predicted to be proportional to the square of electron energy. The data for ^{14}C (Fig. 5 *C*) exhibited an ~80-fold greater Bremsstrahlung intensity than the ^3H data, in agreement with the ~9-fold difference in their average initial electron energies.

[2] The Bremsstrahlung radiation intensity, I (number of photons · energy per photon), for monoenergetic beta particles in thin targets is constant for all photon energies, $h\nu$, up to $h\nu = E_{max}$ (beta), where it drops abruptly to zero (Evans, 1955). This constant intensity results in greater numbers of photons at lower photon energies. In thick targets, progressive absorption of beta energy presents each successive layer of absorbent with beta particles having lower initial energy (or effective E_{max}). This further skews the distribution of Bremsstrahlung photons toward lower energies. The energy spectrum for a continuous beta source is also skewed toward lower initial energies. The combined effect of these factors is that greater numbers of photons at lower energies are produced by beta sources in thick absorbers. Total Bremsstrahlung intensity, I_{tot}, for monoenergetic sources in thick targets is determined by integrating $dI = kZ(\nu_{max} - \nu)\,d\nu$ over all frequencies from ν = 0 to E_{max}/h, where k is a constant, Z is the atomic number of the absorber, and E is the initial beta energy giving $I_{tot} = kZE^2$ per incident beta particle. For continuous beta sources, $I_{tot} = kZE^2_{rms}$, where E_{rms} is the root-mean-square energy for the beta spectrum.

TABLE 1 **Effect of solvent on radioluminescence signals**

Fluorophore solvent	DPH	Terphenyl	Tryptophan
Ethanol	345 ± 12	—	132 ± 1.9
Butanol	2,500 ± 27	262 ± 21	411 ± 3.4
Heptane	13,900 ± 510	33,300 ± 980	—
Toluene	150,000 ± 8,600	680,000 ± 10,000	—

Average fluorophore concentrations were 300, 100, and 30 μM for tryptophan, DPH, and terphenyl, respectively. ^{3}H-palmitic acid or ^{3}H-cholesterol concentrations averaged 35 μCi for ethanol, butanol, and heptane solutions. For toluene, the radioisotope concentration was diluted 1:49 to reduce the high signal from scintillation. Values are in cps (mean ± SD) for triplicate determinations. Radioluminescence measurements were carried out in 0.5 ml samples and are given as L_{rad} (cps/μmol fluorophore/μCi of radioisotope. Data are corrected for background (solvent without fluorophore), fluorophore quantum yield, photomultiplier quantum efficiency, and inner-filter effect.

It was assumed in the theoretical development that the probability for fluorescence excitation is proportional to the local density of deposited energy (keV/cm^3). A major testable prediction of this assumption is that for equal fluorophore concentrations and equal μCi quantities of different radioisotopes dissolved in water, the radioluminescence signal should be proportional to the average density of electron energy deposition. This prediction is supported by the SPR data given in Fig. 5 *A*. With correction for fluorophore concentration, radioisotope activity, and average initial electron energy, the ^{3}H and ^{14}C SPR signals from fluorescein were in excellent agreement in magnitude and shape. This relationship has also been observed in electron-impact absorption spectroscopy where spectral intensity, measured as incident electron current and energy, is proportional to deposited energy density (Lassettre and Francis, 1963).

An important factor influencing the excitation of a fluorophore by an electron is the physical properties of the surrounding media. This "scintillant" effect (Horrocks, 1974) arises from the ability of solvent molecules to effectively capture and transfer energy to a fluorescent molecule which may not lie directly along the path of the electron. Whereas water and ethanol have little or no scintillant effect, aromatic organic solvents have a strong scintillant effect. Hydrocarbon solvents that contain no double bonds have been reported to have moderate scintillant effects (Hirayama and Lipsky, 1971). Table 1 shows data for three fluorophores in several solvents. The fluorophores diphenylhexatriene (DPH) and terphenyl give progressively higher signals as the solvent "scintillant" strength increases from butanol to heptane to the aromatic compound toluene. Tryptophan dissolved in butanol gives higher signals than that in ethanol in which scintillant effects are minimal. Because scintillant effects influence the SPR signal, they must be avoided or taken into account for quantitative distance measurements (see accompanying manuscript).

The $D_x(R)$ curves shown in Figs. 3, *D* and *E* make testable predictions about the radioluminescence signal measured for specified distances between radioisotope and fluorophore. The prediction for ^{14}C was tested experimentally. ^{14}C-palmitic acid and 12 (9-anthroyloxy) stearic acid were dissolved in separate solutions containing PVC and applied to glass coverslips by dipping. Coverslips coated with thin films of PVC containing ^{14}C or fluorophore were separated by a layer of water whose average thickness was determined from the volume of water and the surface area of the layer. Fig. 6 shows the dependence of radioluminescence signal on ^{14}C-to-fluorophore distance. The data show a decrease in SPR signal with increasing distances between the ^{14}C and fluorophore layers. A regression of the ^{14}C point-to-plane energy density curve to this data shows good agreement with the theoretical predictions of the Monte Carlo calculation.

DISCUSSION

This paper establishes a theory for the origin and interpretation of single photon radioluminescence signals in aqueous media. The spatial distribution of energy deposited by beta electrons was determined by a Monte Carlo calculation which averaged the energy deposition profiles of many electrons moving along randomly selected trajectories. The energy deposition profile was related to

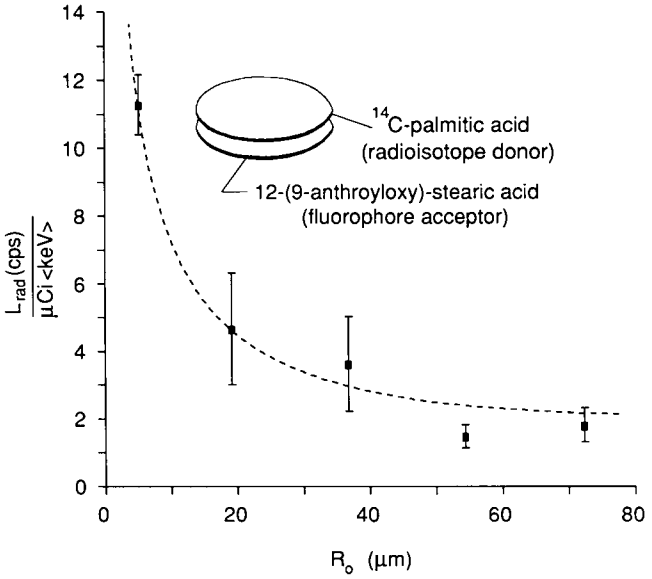

FIGURE 6 Experimental validation of the predicted distance dependence for decay of ^{14}C. Radioluminescence signals (mean cps · μCi^{-1} · $\langle$keV$\rangle^{-1}$, ±SD) were measured for PVC-coated glass coverslips separated by an aqueous layer at four specified thicknesses and a measurement without the aqueous layer. The PVC coatings, *f*, as shown schematically in the inset, contained ^{14}C-palmitic acid at ~0.9 μCi/coated surface or 12-(9-anthroyloxy)-stearic acid at ~50 nmol/coated surface (see Methods). The dashed curve is the predicted signal for plane-to-plane geometry from Monte Carlo calculations.

excitation of fluorescent molecules by empirical measurements made on a series of fluorophores in different solvents. The predicted distance dependence for fluorescence excitation by ^{14}C beta decay was validated experimentally. The calculations and experimental results indicate that single photons produced by radiation-induced excitation of common fluorescent molecules are measurable and give useful information about the geometric relationship between "donor" radioisotope and "acceptor" fluorophore.

Radioluminescence phenomena occur in principle for radioisotope decay producing alpha particles, electrons, positrons, and/or gamma rays. For relevant biological distances, however, donors that are low energy pure beta emitters with high specific activity (^{3}H, ^{14}C, and ^{35}S) provide the most useful and unambiguous distance information. Other potentially useful isotopes in radioluminescence measurements are ^{36}Cl and ^{131}I. SPR measurements with ^{36}Cl and fluorescein showed an emission peak that was similar in shape to those observed in Fig. 5 *A* with excitation by ^{3}H and ^{14}C. However, the signal magnitude was greater than that predicted theoretically because of additional fluorophore excitations from other modes of ^{36}Cl decay including pair annihilation and electron capture (Kocher, 1981). These diverse and delocalized sources of excitation energy significantly complicate the determination of donor-acceptor separation. The important characteristics of the fluorophore acceptor are high molar absorbance and quantum yield, and a fluorescence emission spectrum that falls in a wavelength range of high photomultiplier sensitivity. Finally, the generation of a radioluminescence signal requires proximity between the radioactive donor and fluorescent acceptor; for electrons produced by ^{3}H, distances of up to 0.5–1 μm are in principle measurable, whereas with ^{14}C and ^{35}S, it should be possible to measure larger distances of up to 5–10 μm.

The Monte Carlo simulation provided quantitative information about the spatial distribution of electron energy deposition by tracking thousands of phantom electrons with different initial energies through multiple random scattering events. Similar general calculations have been performed for estimation of the energy deposited by electron beams in various materials for applications in microbeam analysis and radiation therapy (Almond, 1976). Our model for deposition of energy by low energy electrons in aqueous media gave each electron the same initial direction and tracked its full three-dimensional trajectory. The resultant energy distribution function, in units of keV/cm^3, together with information about the cross-section for fluorescence excitation, was used to predict radioluminescence signals for specified radioisotope-fluorophore geometries. The continuous-slowdown approximation used in the model replaces a small number of energy losses from high energy interactions by an average electron energy loss over distance. The Bethe equation used in the Monte Carlo calculations (Eqs. 1 and 2) is based on the Bohr approximation which assumes that the incident beta electron may interact with all orbital electrons in the absorbing medium. This is rigorously valid only for beta electrons for which $2\pi e^2/h\beta c \ll 1$, where e is the electrostatic charge of the electron (Bethe and Ashkin, 1953). When this condition is not met, the beta electrons only interact with atomic electrons in outer orbitals and Eqs. 1 and 2 are no longer strictly valid. For this reason the calculation for each electron trajectory was terminated when electron energy declined to 0.5 keV. There is little further penetration by electrons with energy < 0.5 keV, so that termination of the calculation had no significant effect on the energy distribution profiles.

The Monte Carlo simulation provides a prediction of the three-dimensional electron scattering distribution for beta electrons at a series of energies for different isotopes and absorbing media. Validation of the scattering pattern produced by the Monte Carlo simulation comes from studies of energy deposition in plastic by monoenergetic electron beams (Goldstein et al., 1981). In these studies, chemical etching of plastics that have been irradiated by an electron beam, gave visible patterns related to the density of energy deposition that were in good agreement with theory. The general shape of the contours from the Monte Carlo calculation in our study (Fig. 2) are similar to those measured experimentally by the etching of radiated polymethylmethacrylate (Goldstein et al., 1981).

There was good correlation between the efficiency for fluorophore excitation by beta electrons and fluorophore molar absorbance. This simple relationship is important in the design and quantitative interpretation of radioluminescence experiments performed in a nonscintillant environment. The relationship between fluorophore excitation and molar absorbance is consistent with the view that the deposited electron energy rapidly dissipates into compartments with progressively smaller energies by a number of physical processes including electronic excitation, ionization and recapture, and production of secondary electrons (Bethe and Ashkin, 1953). The deposited electron energies are in the keV range, whereas fluorophore excitation requires only 3–5 eV. Thus, it is likely that the appropriate energies for fluorophore excitation from S_0 to S_1 are produced by the dissipation of higher energies in the local environment of the fluorophore rather than by direct beta-fluorophore collision. Support for this hypothesis comes from work in electron-impact spectroscopy and liquid scintillation spectrometry. The agreement in Figs. 5, *A* and *B* between fluorophore emission spectra produced by electron-impact and photon excitation strongly suggests that selection rules and oscillator strengths were the same for these two modes of excitation. This correspondence is strongest when the fluorophore transition energy is small compared with the energy of the incident electron (Lassettre and Francis, 1963). In liquid scintillation spectros-

copy, the probability of electron-impact excitation for different energy transitions of solvent molecules is proportional to their optical extinction coefficients (Horrocks, 1974). Thus the cross-sections for excitation in electron-impact and photon excitation are closely related, supporting the correlation found between the SPR cross-section (σ_F) and the integrated fluorophore absorption spectrum (Fig. 4). Another prediction of this proposed physical mechanism is that the probability for fluorophore excitation is proportional to the density of local energy deposition. This is supported by the data in electron-impact spectroscopy where detected intensity is proportional to the intensity of the incident electron beam (Lassettre and Francis, 1963). In our work, experimental validation for this prediction is provided by the observation that equal μCi quantities of ^{3}H and ^{14}C produce radioluminescence signals that are proportional to the average electron energy density in the sample. In Fig. 5 *A*, the magnitude of ^{3}H and ^{14}C radioluminescence signals for fluorescein are nearly equal after correction for this 8.75-fold energy difference.

The theory provides evidence that radioluminescence signals should be measurable in a variety of novel biological applications. Several applications, including ligand-receptor binding, lipid exchange kinetics, and membrane transport, make use of the radioisotope-fluorophore proximity requirement without model-dependent quantitative determination of distances. The quantitative model is required for radioisotope-fluorophore distance determination in fixed geometries such as that between membrane proteins or between an intracellular protein and the cell plasma membrane. In an ideal experimental apparatus in which $I_a(\lambda)Q_yGQ_e(\lambda) = 1$, the theory predicts a radioluminescence signal of 1,220 cps from 50 μCi of ^{3}H labeled molecules, each bound at a distance of 10 nm from single fluorescein fluorophores; at 25 nm, the predicted signal is 170 cps and at 100 nm it is 7.5 cps. The predicted signals are ~5-fold greater at these distances for excitation by ^{3}H due to the shorter penetration depth of ^{3}H. In water, the energy density produced by ^{14}C electron exceeds that from ^{3}H electrons beyond ~1.2 μm. Thus, notwithstanding their greater Bremsstrahlung production, higher energy radioisotopes such as ^{14}C are superior to ^{3}H for SPR measurements of long distances.

There are a number of factors to consider in the application of radioluminescence. The use of relatively large quantities of radioisotopes may be required. The single photon signals are very small, requiring the construction of specialized detection instrumentation. Optical cut-on or interference filters may be used to improve the signal-to-background ratio by passing the emission peak of the fluorophore while blocking portions of the broad Bremsstrahlung emission spectrum. For distance measurements, because of the $\sim 1/R_0^2$ dependence of signal on distance, the radioluminescence method extends remarkably the ability to measure submicroscopic distances compared with conventional fluorescence energy transfer. However, if there is a distribution of donor-acceptor distances, the radioluminescence method gives only a weighted averaged distance, whereas fluorescence life-time analysis can in principle provide information to evaluate distance distributions. In addition, because of the small signal size, it is generally not practical to obtain spatial information from SPR with subcellular resolution by microscopy imaging methods. Other practical considerations for measurement of radioluminescence phenomena in biological samples are evaluated in the accompanying experimental manuscript.

We thank Drs. James Abney, Bethe Scalettar, and N. Periasamy for help in the theoretical development and for critical reading of the manuscript, and Dr. S. M. Seltzer for helpful discussion about the physics of electron energy absorption.

This work was supported by grants DK16095, DK43840, DK35124, HL42368, and DK39354 from the National Institutes of Health and by a grant-in-aid from the W. Duncan MacMillan Trust. Dr. Bicknese was supported by NRSA grand GM15145. Dr. Verkman is an established investigator of the American Heart Association. This is publication number 121 of the MacMillan-Cargill Hematology Laboratory.

Received for publication 2 March 1992 and in final form 20 July 1992.

REFERENCES

Almond, P. R. 1976. Radiation physics of electron beams. *In* Clinical Applications of the Electron Beam. Norah duV. Tapley, editor. John Wiley & Sons, New York. 7–80.

Berger, M. J. 1963. Monte Carlo calculation of the penetration and diffusion of fast charged particles. *In* Methods in Computational Physics, V. 1. B. Alder, S. Fernbach, and M. Rotenberg, editors. Academic Press, New York. 135–213.

Berger, M. J., and S. M. Seltzer. 1982. Tables of energy-deposition distributions in water phantoms irradiated by point-monodirectional electron beams with energies from 1 to 60 MeV, and applications to broad beams. NBSIR 82-2451, National Bureau of Standards. 1–54.

Bethe, H., and J. Ashkin. 1953. Passage of radiations through matter. *In* Experimental Nuclear Physics. E. Segre, editor. John Wiley & Sons, Inc., New York. 166–357.

Blanchard, C. H., and U. Fano. 1951. A formula for multiple scatter electrons. *Phys. Rev.* 82:767.

Bosworth, N., and P. Towers. 1989. Scintillation proximity assay. *Nature (Lond.)* 341:167–168.

Demas, J. N. 1983. Excited State Measurements. Academic Press, New York. 213–215.

Evans, R. 1955. The Atomic Nucleus. McGraw-Hill Book Company, Inc., New York. 536–631.

Goldstein, J. I., D. E. Newbury, P. Echlin, D. C. Joy, C. Fiori, and E. Lifshin. 1981. Scanning Electron Microscopy and X-ray Microanalysis. Plenum Press, New York. 53–72.

Hirayama, F., and S. Lipsky. 1971. Saturated hydrocarbons as donors in electronic energy transfer processes. *In* Organic Scintillators and Liquid Scintillation Counting. Academic Press, New York. 205–221.

Horrocks, D. L. 1974. Applications of Liquid Scintillation Counting. Academic Press, New York. 12–37.

Kocher, D. C. 1981. Radioactive Decay Data Tables, A Handbook of Decay Data for Application to Radiation Dosimetry and Radiological Assessments. Technical Information Center, U.S. Department of Energy, Springfield, MA. p. 71.

Lassettre, E., and S. A. Francis. 1963. Inelastic scattering of 390-V electrons by helium, hydrogen, methane, ethane, cyclohexane, ethylene, and water. *J. Chem. Phys.* 40(5):1208–1217.

Marion, J. B. 1971. Classical Dynamics of Particles and Systems. Academic Press, New York. 384–385.

Mladjenovic, M. 1973. Radioisotope and Radiation Physics. Academic Press, New York. 124–125.

Renschler, C. L., and R. L. Clough. 1989. Demonstration of completely organic, optically clear radioluminescent light. *J. Appl. Phys.* 66(9):4542–4544.

Rossi, B. 1952. High-Energy Particles. Prentice-Hall, Inc., Englewood Cliffs, NJ. 55–56.

Shahrokh, Z., S. Bicknese, S. B. Shohet, and A. S. Verkman. 1982. Single photon radioluminescence. II. Signal detection and biological applications. *Biophys. J.* 63:1267–1279.

von Tscharner, V. V., and G. K. Radda. 1980. A study of changes in surface area and molecular interactions in phospholipid vesicles by condensed phase radioluminescence. *Biochim. Biophys. Acta.* 601:63–77.

von Tscharner, V. V., and G. K. Radda. 1981. The effect of fatty acids on the surface potential of phospholipid vesicles measured by condensed phase radioluminescence. *Biochim. Biophys. Acta.* 643:435.